HIV-1 matrix-31 membrane binding peptide interacts differently with membranes containing PS *vs.* PI(4,5)P$_2$

Lauren O'Neil [a], Kathryn Andenoro [a], Isabella Pagano [a], Laura Carroll [a], Leah Langer [a], Zachary Dell [a], Davina Perera [b], Bradley W. Treece [a], Frank Heinrich [a,c], Mathias Lösche [a,c,d], John F. Nagle [a], Stephanie Tristram-Nagle [a,*]

[a] Biological Physics Group, Physics Department, Carnegie Mellon University, Pittsburgh, PA 15213, United States
[b] Biomedical Engineering, Douglass College, Rutgers University, New Brunswick, NJ 08901, United States
[c] National Institute of Standards and Technology Center for Neutron Research, Gaithersburg, MD 20899, United States
[d] Biomedical Engineering, Carnegie Mellon University, Pittsburgh, PA 15213, United States

ABSTRACT

Efficient assembly of HIV-1 at the plasma membrane (PM) of the T-cell specifically requires PI(4,5)P$_2$. It was previously shown that a highly basic region (HBR) of the matrix protein (MA) on the Gag precursor polyprotein Pr55^{Gag} is required for membrane association. MA is N-terminally myristoylated, which enhances its affinity to membranes. In this work we used X-ray scattering and neutron reflectivity to determine how the physical properties and structure of lipid bilayers respond to the addition of binding domain peptides, either in the myristoylated form (MA$_{31}$myr) or without the myristoyl group (MA$_{31}$). Neutron reflectivity measurements showed the peptides predominantly located in the hydrocarbon interior. Diffuse X-ray scattering showed differences in membrane properties upon addition of peptides and the direction of the changes depended on lipid composition. The PI(4,5)P$_2$-containing bilayers softened, thinned and became less ordered as peptide concentration increased. In contrast, POPS-containing bilayers with equivalent net charge first stiffened, thickened and became more ordered with increasing peptide concentration. As softening the host cell's PM upon contact with the protein lowers the free energy for membrane restructuring, thereby potentially facilitating budding of viral particles, our results suggest that the role of PI(4,5)P$_2$ in viral assembly goes beyond specific stereochemical membrane binding. These studies reinforce the importance of lipids in virology.

© 2016 Elsevier B.V. All rights reserved.

1. Introduction

Retroviral particle production occurs at the infected cell's plasma membrane (PM) where the virus acquires its lipid envelope [1]. Viral production is a complex, multistep process mediated by the viral structural protein Gag [2]. Human immunodeficiency virus (HIV-1) Gag is synthesized as a precursor polyprotein, Pr55^{Gag}, which, upon viral release, is cleaved into four major domains: N-terminal matrix (MA), capsid (CA), nucleocapsid (NC) and P6 [3]. MA protein binds Gag to the plasma membrane (PM), CA forms a Gag dimerization interface, NC promotes multimerization of Gag through binding to RNA, and P6 recruits the ESCRT cellular protein complexes (endosomal-sorting complex required for transport) that are required for viral release [2]. Both MA and NC are highly basic proteins, and can thus potentially bind to acidic membranes and nucleic acids in the cell. Small-angle

neutron scattering suggested that in full-length Gag, the MA and NC domains are closely juxtaposed in solution, resulting in a compact, folded-over protein [4]; this was confirmed using single molecule-Förster resonance energy transfer [5]. In the absence of nucleic acid, a similar conformation of Gag was observed by neutron reflectivity on negatively charged membranes, but upon increasing nucleic acid concentration, the Gag protein assumed the elongated shape that persists in the immature virus [6]. Whereas it is established that the nucleocapsid (NC) domain of Gag specifically recognizes motifs in the viral RNA genome for packaging [7,8], there is compelling evidence that the matrix (MA) domain also binds to cellular RNA [9–11].

Membrane binding of HIV-1 Gag depends on a conserved highly basic region (HBR) between amino acids 19 and 31 [12,13] in the 131 amino acid MA protein as well as on the myristoyl moiety at MA's N-terminus. In solution the myristate moiety is sequestered within the MA globular domain, but a conformational switch exposes it, enhancing membrane binding [14]. The HBR contributes to the conformational switch by interacting with acidic phospholipids on the inner leaflet of the PM [12,14]. Myristoylation occurs co-translationally, where the

14-carbon saturated fatty acid, myristic acid, is attached to the N-terminal glycine that is exposed after the first methionine is removed. Mutating the N-terminal glycine to alanine reduces membrane binding and inhibits virus release [15,16]. Mutating the 2nd to 5th residues after glycine also reduces membrane binding and virus particle production, indicating that these residues are required for N-myristoyltransferase recognition [16–18]. Thin section electron microscopy has more recently shown that the G2A mutation causes roughly spherical particles to assemble within the cytoplasm [19].

Targeting of Gag to the PM occurs by interaction between the MA HBR and phosphatidylinositol (4,5)–bisphosphate (PI(4,5)P$_2$ or PIP$_2$), which is concentrated primarily on the cytoplasmic leaflet of the PM. Mutant studies demonstrated that PM PIP$_2$ is required for efficient HIV-1 viral release [20], and for avoiding misdirection of nascent virions to endosomal compartments [21]. Additional mutant studies revealed that amino acids K17, K29 and K31 are involved in PIP$_2$ binding, while K25 and K26 inhibit PIP$_2$-independent membrane binding of Gag [9]. In a mutant containing the myristoyl group but lacking the HBR, production of viral particles was decreased by 10-fold, and those that formed near the plasma membrane did not contain Envelope proteins (Env) [22]. The requirement for the tetra-anionic PIP$_2$ instead of the mono-anionic negatively charged PS has been intensively investigated. Liposomal studies showed that binding to PC/PS is significantly higher in the presence of small amounts of PIP$_2$, suggesting a specific interaction [23]. Other experimental approaches have been used to demonstrate specific binding of HIV-1 Gag to PIP$_2$ [24–26]. Solution nuclear magnetic resonance (NMR) revealed the structure of myristoylated MA bound to water-soluble PIP$_2$ with truncated (C$_4$ or C$_8$) chains [25]. These studies showed that MA-PIP$_2$ binding promotes myristoyl switching and suggested that the sn-2 acyl chain of PIP$_2$ is inserted into a hydrophobic cleft in MA, with the inositol group packed against the HBR of MA. More recently, the same group has re-examined their previous study, using native PIP$_2$ acyl chains (5%) in DHPC/DMPC bicelles, and found that the PIP$_2$ sn-2 acyl chain does not dissociate from the membrane to bind into a cleft in the MA protein [27].

A recent SPR study examined the role of lipids in membrane binding of the myristoylated and non-myristoylated forms of MA [28] and reported that myristoylation increases MA affinity to PC/PS membranes by factors up to ~20 depending on membrane charge. Cholesterol in PC/PS membranes increased MA affinity only mildly, while it increased it much more in PIP$_2$-containing PC/PS membranes, in particular for the myristoylated protein. This suggests yet another additive effect of MA protein binding, between the myristoyl group and PIP$_2$ [28]. Therefore, membrane binding is a sensitive assay of the contributions of different lipids to the MA protein/membrane interaction; however, binding is only one part of the picture.

In the present work, we quantify interactions between the HIV-1 Gag MA membrane binding interface with lipid bilayers and use X-ray diffuse scattering to study the effect of binding on membrane bending rigidity, chain order, area/lipid and bilayer thickness. In order to focus on the membrane binding domain, we investigate the N-terminal 31 AA residues of MA that include the myristoylation site (G2) and the HBR (AAs 20–32). Numbering begins with G2, since the N-terminal methionine (M1) is removed during protein synthesis. The model peptide, henceforth called MA$_{31}$myr, includes the main membrane interaction sites, myristoyl and the HBR, of the full-length MA protein. For contrast we also study MA$_{31}$ without the myristoyl group. These peptides are reductionist proxies to explore the molecular interactions between the membrane binding interface and bilayers with different lipid headgroups. We quantify how bilayers respond to such interactions with MA$_{31}$myr and MA$_{31}$, and reveal significant differences between peptide interactions with PIP$_2$ and PS-containing membranes. Importantly, the observed differences in physical response make PIP$_2$-containing bilayers more susceptible to membrane reorganization than bilayers devoid of PIP$_2$, and thereby facilitate viral budding.

2. Materials and methods

2.1. Lipids and peptides

Synthesized, lyophilized lipids were purchased from Avanti Polar Lipids (Alabaster, AL) and used as received, and HPLC grade organic solvents were purchased from Sigma/Aldrich. Lipid structures are shown in Fig. 1. Membrane mimics were prepared by first dissolving lyophilized lipids in chloroform (POPC) or hexafluoroisopropanol HIP (POPS, POPE, inositol lipids) and then mixing these stock solutions to create the lipid mole ratio compositions: POPC/POPS (92:8, 60:40), POPC/PIP$_2$ (98:2, 95:5, 90:10, 80:20), POPC/POPE (50:50), POPC/POPE/POPS (46:46:8), POPC/POPE/PIP$_2$ (49:49:2, 50:30:20), POPC/POPE/PI (50:30:20), POPC/POPE/PIP (50:30:20), POPC/POPE/POPS/Chol (31:31:8:30), POPC/POPE/PIP$_2$/Chol (34:34:2:30) and POPC mixtures with PI or PIP (95:5, 90:10, 80:20). Myristoylated-MA$_{31}$ (MA$_{31}$myr) and MA$_{31}$ (see Fig. 1 for structure) were purchased from the Peptide synthesis Facility (University of Pittsburgh, Pittsburgh, PA); mass spectroscopy indicated >95% purity. These matrix peptides correspond to amino acid residues 1–31 of the 131 residues in the MA protein [29]. MA$_{31}$myr was dissolved in HIP to form mole fractions in lipids between 0.002 and 0.020. The molecular weight of MA$_{31}$ (4289) and MA$_{31}$myr (4499) included 7 trifluoroacetate counterions from the peptide synthesis. Solvents were removed by evaporation in the fume hood, followed by 2 h in a vacuum chamber at room temperature. In this work, lipid mixtures will be represented by mole ratios, while peptide/lipid mixtures will be represented by mole fractions. Sample preparations will be represented by mg/ml.

2.1.1. Samples for X-ray scattering

4 mg of dried lipid/peptide mixture was re-dissolved in 200 μl HIP, or chloroform:HIP (4:1 or 1:1, vol:vol) ratios for most of the lipid compositions. These mixtures were plated onto silicon wafers (15 × 30 × 1 mm) via the rock and roll method [30] to produce stacks of ~1800 well-aligned bilayers; solvents were removed by evaporation in the fume hood, followed by 2 h under vacuum at room temperature. Samples were prehydrated in polypropylene hydration chambers at 37 °C for 1–6 h directly before hydration in a thick-walled X-ray hydration chamber [31] for 0.5–1 h.

2.1.2. Samples for neutron reflectivity

10 mg lipid mixtures, POPC/POPS (60:40) or POPC/PIP$_2$ (90:10), were prepared as in Section 2.1. MA$_{31}$ or MA$_{31}$myr was dissolved in HIP and added to the lipid mixtures in mole fractions: 0.01, 0.0125 and 0.01667. Organic solvent was removed by evaporation in the fume hood and then under vacuum for 12 h. Samples were stored at −20 °C until shortly before the neutron reflectivity measurements. Dried peptide/lipid films were rehydrated in a 1 M NaCl aqueous solution to a final concentration of 5–6 mg/ml and bath sonicated for 60–90 min until the vesicular suspension became transparent. Self-assembled monolayers (SAMs) of HC18 tethers were formed on 3″ diameter silicon wafers as previously described [32]. Sparsely-tethered bilayer lipid membranes (stBLMs) were formed by exposing the SAM to the vesicle suspension for 60 min in a NIST reflectivity flow cell, followed by a rinse with 40 ml deionized water [28].

2.1.3. Samples for densimetry

Multilamellar vesicles (MLVs) were prepared by mixing dried lipid/peptide mixtures with MilliQ water to a final concentration of 5–100 mg/ml in nalgene vials and cycled three times between −20 °C and 50 °C for 10 min at each temperature with intermittent vortexing [33]. Pure MA$_{31}$ and MA$_{31}$myr were dissolved in MilliQ water at 1–5 mg/ml and vortexed to dissolve.

POPC

POPE

POPS

PI

PIP

PIP$_2$

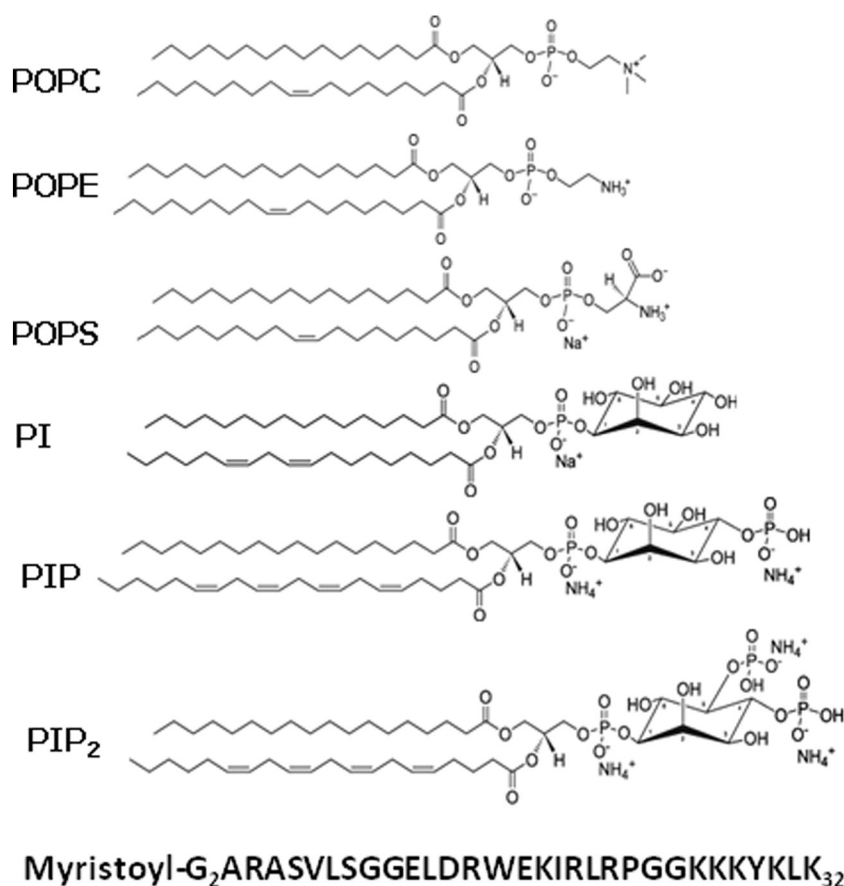Myristoyl-G$_2$ARASVLSGGELDRWEKIRLRPGGKKKYKLK$_{32}$

Fig. 1. Structures of lipids used in this work (from Avanti Polar Lipids WEBsite). Lipid names: POPC, palmitoyloleoylphosphatidylcholine; POPE, palmitoyloleoylphosphatidylethanolamine; POPS, palmitoyloleoylphosphatidylserine; PI, phosphatidylinositol (soy); PIP, phosphatidylinositol-4-phosphate (porcine brain); phosphatidylinositol-4,5-bisphosphate (porcine brain). The primary structure of MA$_{31}$myr is shown. Counterions are shown for the charged lipids.

2.1.4. X-ray scattering. LAXS

Oriented stacks of membrane mimics, ~1800 layers, were hydrated through the vapor phase. Low-angle X-ray scattering from these samples at 37 °C were obtained at the Cornell High Energy Synchrotron Source (CHESS) using previously described methods [34,35] using X-ray wavelengths 1.187, 1.177 and 1.108 Å on three separate CHESS trips, and sample-to-detector S-distances 377, 373 and 387 cm at the G1 station. The analysis of diffuse LAXS from oriented stacks of fluctuating fluid bilayers has been previously described [31]. Form factors $|F(q_z)|$ and bending moduli K_C were obtained as previously described [34,36,37]. When peptides are added, K_C is an effective bending modulus that accounts for traditional bending of a homogeneous bilayer, ignoring a tilt mode and any local disordering effect of the peptides on the height-height pair correlation functions [38].

2.1.5. WAXS

Wide-angle X-ray scattering data from the same samples as for LAXS were obtained at a fixed angle of 0.5°, background collected at −0.5° was subtracted, and these data were analyzed to obtain the S_{xray} order parameter as described in Ref. [39]. S-distances for WAXS were 145, 142 and 163 cm.

2.2. Neutron reflectivity

NR measurements were performed at the NGD-MAGIK reflectometer [40] at the NIST Center for Neutron Research over a momentum transfer range 0–0.25 Å^{-1}. Three bulk contrasts were used: D$_2$O, H$_2$O and a 2:1 mixture by volume of D$_2$O and H$_2$O (CM4). 6 h scans at

37 °C were performed for each solvent contrast. The 1D-structural profile along the lipid bilayer normal was modeled using a composition-space model as described in Ref. [41].

2.3. Densimetry

Volumes of peptides in water and in MLVs were determined at 37 ± 0.01 °C using an Anton-Paar USA DMA5000M (Ashland, VA) vibrating tube densimeter [42].

3. Results

3.1. Low-angle X-ray scattering (LAXS)

3.1.1. Intensity data

Synchrotron LAXS data are shown in Fig. 2A, B, C for POPC, POPC/0.02 MA and POPC/0.02 MAmyr, respectively. The lobes of diffuse scattering result from fluctuational disorder that occurs spontaneously in fully hydrated, oriented bilayers. Analysis of the weak arcs emanating from the diffuse, white lobes [43] indicates a small mosaic spread (i.e., an excellent bilayer alignment) with mosaic spread <1 degree. Although visual comparison shows only small differences between the lobes of diffuse scattering data in Fig. 2A, B and C, when their intensities in the q_r direction are plotted (Fig. 2D), one sees that POPC is the most narrow, POPC/MA$_{31}$myr slightly wider, while POPC/MA$_{31}$ has the largest width. The widths of the intensity lobes are one indication that POPC/MA$_{31}$ causes the greatest softening of the POPC membrane, which is quantified by determining the bending modulus, K_C (see Section 3.1.2).
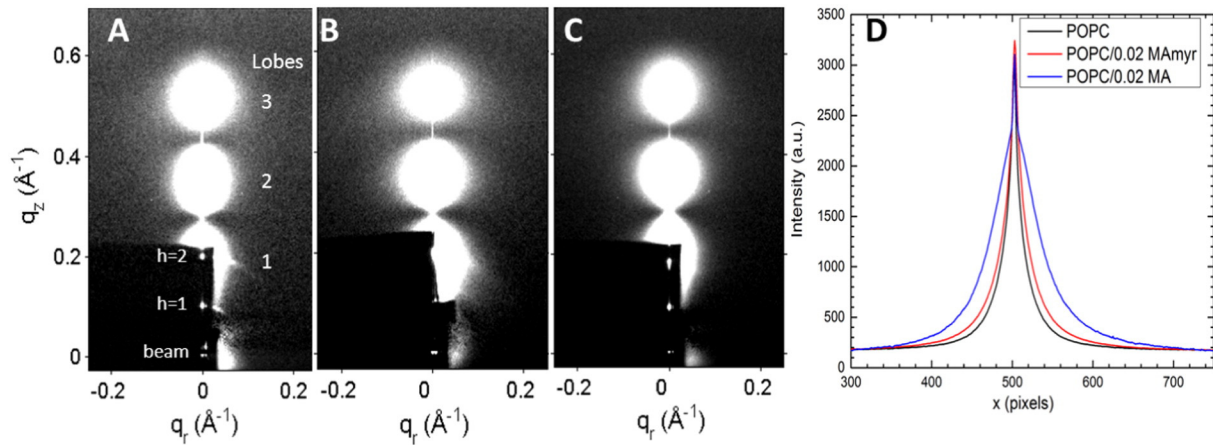
Fig. 2. 2D CCD images of hydrated LAXS intensity (white is most intense) at 37 °C where z is the direction of the membrane normal and r is the in-plane direction. (A) POPC, (B) POPC/0.02MA$_{31}$, and (C) POPC/0.02MA$_{31}$myr. Lamellar D-spacings corresponding to these images are 62.6 Å, 67.3 Å and 74 Å for A, B and C, respectively. Diffuse scattering lobes (1–3) are identified with large numbers. The dark rectangle in the lower left corner is due to molybdenum sheets that attenuate the beam and the h = 1, 2 lamellar diffraction peaks. (D) X-ray intensity vs. lateral x pixels collected with a broad, horizontal slice through lobes 2 and 3.

3.1.2. Bending moduli

Larger fluctuations indicate lower resistance of the membrane to bending, resulting in a lower effective bending modulus, K_C. K_C results for the three samples shown in Fig. 2 appear as the black solid squares in Fig. 3A. This quantitative data analysis [34] confirms greater fluctuations (52% smaller K_C) in the POPC sample containing 0.02 of the non-myristoylated MA$_{31}$, while K_C for 0.02 MA$_{31}$myr/POPC was only slightly smaller compared to peptide-free POPC. When either peptide at 0.02 mol ratio was mixed with POPC/PIP$_2$ (80:20), Fig. 3A shows that K_C decreased much more from the control POPC/PIP$_2$ value than the decrease when the peptides were added to POPC. This indicates that the interaction of the peptides with the membrane is greatly enhanced by the electrostatic interaction between the positively charged peptides and the negatively charged membrane.
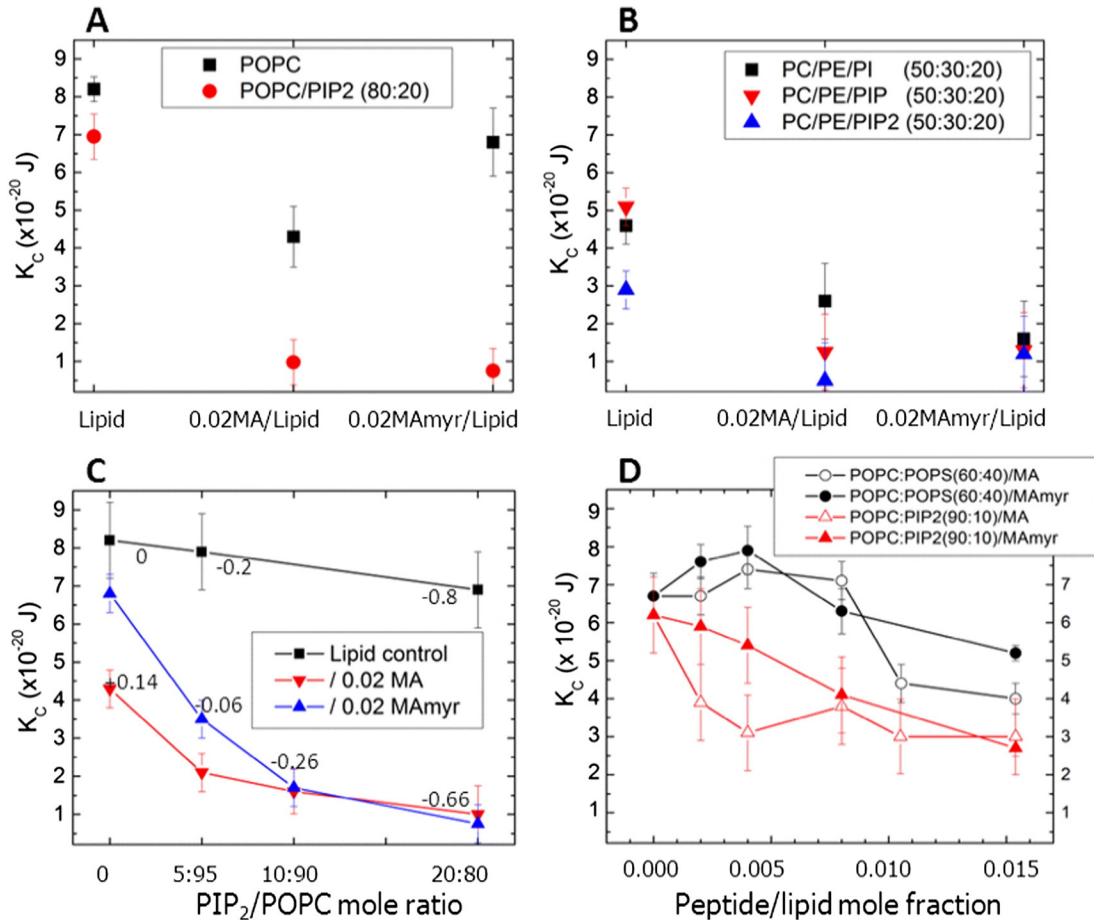

Fig. 3. Bending modulus, K_C, as a function of lipid and peptide concentration. (A) 0.02 MA$_{31}$ or MA$_{31}$myr in POPC, in POPC/PIP$_2$ (80:20), (B) 0.02 MA$_{31}$ and MA$_{31}$myr in POPC/POPE/PI (50:30:20), in POPC/POPE/PIP (50:30:20), in POPC/POPE/PIP$_2$ (50:30:20), (C) 0.02 MA$_{31}$ or MA$_{31}$myr in POPC with increasing PIP$_2$, (D) Increasing MA$_{31}$ or MA$_{31}$myr in POPC/POPS (60:40) or POPC/PIP$_2$ (90:10). Numbers in Fig. 3C indicate the net membrane charge/lipid plus protein. Lipid control indicates samples with no peptides. Error bars represent standard deviations of the average K_C values from 2 to 5 different samples.

In panel B the PC headgroup was partially replaced with the smaller PE headgroup that gives a negative spontaneous curvature to monolayers. For the lipid mixtures without peptides, the partial replacement of PC with PE decreased K_C, indicating that a lipid with negative curvature softens the bilayer. When the negatively charged lipids PI, PIP or PIP_2 were added to the PC/PE mixture, K_C decreased further, as with POPC. While systematic studies of lipid asymmetry in T-cells have not been performed to our knowledge, in red blood cells there is at least as much PE as PC in the cytoplasmic leaflet of the plasma membrane [44,45]. Therefore we have included PE in several samples in this work.

Differences between MA_{31} and $MA_{31}myr$ occur at low concentrations of PIP_2 as shown in Fig. 3C; non-myristoylated MA_{31} caused a greater decrease in K_C than did $MA_{31}myr$, similar to their difference with neutral POPC (Fig. 3A). The difference in K_C between MA_{31} and $MA_{31}myr$ decreased as the net charge for the peptide-containing samples in Fig. 3C ranged from $+0.14$ to negative values.

In order to test the specificity of the PIP_2 headgroup [46], we compared adding increasing amounts of MA_{31} or $MA_{31}myr$ to two lipid mixtures with the same overall net negative charge: POPC/POPS (60:40 mol ratio) and POPC/PIP_2 (90:10 mol ratio) (both -0.4 e per lipid). Fig. 3D shows that increasing amounts of both peptides stiffen at low concentration, and then soften POPC/POPS membranes at higher concentration, yet both peptides monotonically soften POPC/PIP_2 membranes with increasing concentration. The net charge on these samples was dominated by the high concentrations of PIP_2 or PS, ranging from -0.4 to -0.29 per lipid plus protein (see Table 1).

In summary for this subsection, when the net charge was more positive than -0.26 e per lipid, MA_{31} lowered K_C to a greater extent than did $MA_{31}myr$. When the net charge was more negative than $-0.26e$ per lipid, there was little difference in K_C between $MA_{31}myr$ and MA_{31}. With no added peptides, PS and PIP_2 caused a decrease in K_C compared to the POPC control (compare POPC in Fig. 3A with 0 peptide concentration in Fig. 3D). MA_{31} softens membranes more than $MA_{31}myr$ in PIP_2-containing membranes unless the net negative charge exceeds -0.26, and then both peptides soften similarly. Fig. 3D shows that MA_{31} and $MA_{31}myr$ both stiffen at low concentration and then soften at high concentration PS-containing membranes, while both peptides soften PIP_2-containing membranes at all concentrations, yet their overall net charge is identical. Inclusion of POPE in these lipids mixtures (Fig. 3B) decreased K_C; PIP and PIP_2 decreased K_C to a greater extent than PI when combined with POPC and POPE, due to their greater negative charges.

3.1.3. X-ray form factors and electron density profiles

Fig. 4A shows that the form factor of the neutral lipid, POPC, moves to higher q_z upon addition of peptide; this q-space result qualitatively indicates a membrane thinning that is slightly greater for $MA_{31}myr$ compared to MA_{31}. The real-space extent of membrane thinning is indicated in Fig. 4B by comparing the maxima in the total electron density envelope of these three samples. A membrane bilayer thinning of 0.5 Å for POPC/0.02 MA_{31} and 1.2 Å for POPC/0.02 $MA_{31}myr$ occurred, as judged by the peak-to-peak distance.

Fig. 5 shows form factors for MA_{31} and $MA_{31}myr$ as a function of peptide concentration in POPC/POPS (60:40) and POPC/PIP_2 (90:10) lipid membranes. These are the structural results for the samples that yielded the K_C results in Fig. 3D. For increasing peptide concentration in PS-containing membranes, the q_z values decreased and subsequently increased, indicating first a membrane thickening, then a membrane thinning back to the control thickness. Quite differently, in PIP_2-containing membranes, there was an increase in q_z, indicating a membrane thinning that increased with peptide concentration. While these trends are qualitatively revealing, detailed analysis gives the quantitative structural results summarized in Fig. 6A-D. The area/lipid A_L first decreased then increased with added peptides in PC/PS membranes (Fig. 6A), but monotonically increased in PC/PIP_2 membranes (Fig. 6C). Similarly, the hydrocarbon membrane thickness, $2D_C$, first increased and then decreased back to the control value in PC/PS membranes (Fig. 6B), while there was a steady decrease observed in PC/PIP_2 membranes (Fig. 6D). There was no significant difference between MA_{31} and $MA_{31}myr$.

3.2. Wide-angle X-ray scattering (WAXS)

Fig. 7 shows the chain order S_{xray} results as a function of peptide concentration for the series of samples in Fig. 3A. S_{xray} is an order parameter, similar to the NMR order parameter S_{mol} [47], which reports on chain orientational order [39]. The chain order is observed to increase initially and then decrease with increasing concentration of both peptides in POPC:POPS (60:40) membranes. This parallels the trend observed in the structural results for these samples in Fig. 6B; there was first a membrane thickening followed by a membrane thinning at higher peptide concentration. Evidently thickening is due to an increase in chain order which causes the lipid chains to extend, and which reverses at higher concentrations to cause membrane thinning back to the control value. In contrast to POPC/POPS, there was a very gradual decrease in membrane order in the POPC/PIP_2 (90:10) samples, which is consistent with the 2.5 Å membrane thinning that occurred (Fig. 6D). The chain order results are also consistent with the K_C values presented in Fig. 3C for these lipids in that PC/PS lipids first stiffened and then softened with increasing peptide concentration, while PC/PIP_2 lipids generally softened with increasing peptide.

The data above have the advantage of varying charge concentration over a range large enough to more easily see trends. We also obtained results from samples that focused on physiological concentrations of PIP_2. As with the majority of the data shown above, these negatively charged mimics have the same overall net negative charge. Peptide concentration was limited to lipid/0.02 $MA_{31}myr$. Results for K_C, $2D_C$ and area/lipid are given in Table 2, and results for S_{xray} are given in Fig. 8. Addition of the peptide to PIP_2-containing bilayers decreased K_C, consistent with the results in Fig. 3D, decreased the hydrophobic

Table 1
Net charge and D-spacing.

Net charge	Sample	D-spacing result	Sample	D-spacing result
−0.4	Control POPC/POPS (60:40)	D-unbound	Control POPC/PIP2 (90:10)	D-unbound
−0.385	POPC/POPS (60:40)/.002 MA	D-unbound	POPCPIP2 (90:10)/.002 MA	D-unbound
−0.371	POPC/POPS (60:40)/.004MA	D-unbound	POPC/PIP2 (90:10)/.004 MA	D-unbound
−0.34	POPC/POPS (60:40)/.008MA	D-unbound	POPC/PIP2 (90:10)/.008 MA	D-unbound
−0.323	POPC/POPS (60:40)/.011MA	D-unbound	POPC/PIP2 (90:10)/.011 MA	**D-bound**
−0.288	POPC/POPS (60:40)/.015MA	D-unbound	POPC/PIP2 (90:10)/.015 MA	**D-bound**
−0.4	Control POPC/POPS (60:40)	D-unbound	Control POPC/PIP2 (90:10)	D-unbound
−0.385	POPC/POPS (60:40)/.002MAmyr	D-unbound	POPC/PIP2 (90:10)/.002 MAmyr	D-unbound
−0.371	POPC/POPS (60:40)/.004MAmyr	D-unbound	POPC/PIP2 (90:10)/.004 MAmyr	D-unbound
−0.34	POPC/POPS (60:40)/.008MAmyr	D-unbound	POPC/PIP2 (90:10)/.008 MAmyr	D-unbound
−0.288	POPC/POPS (60:40)/.015MAmyr	**D-bound**	POPC/PIP2 (90:10)/.015 MAmyr	**D-bound**

Net charge of the mixtures (peptide plus lipid) is shown in the left-hand column. Samples whose D-spacings continued to increase to large values are described as D-unbound. Samples whose D-spacings continued to decrease or reached a limiting value are described as D-bound.
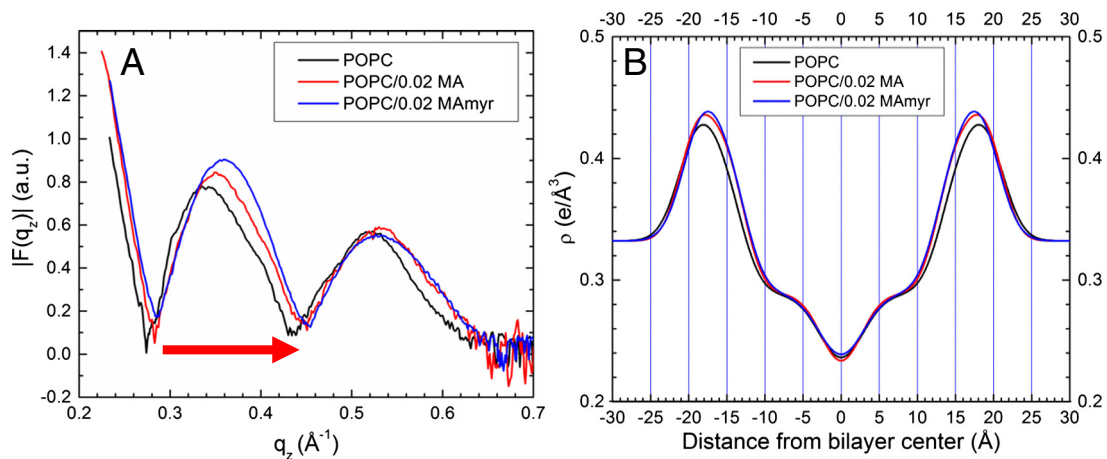
Fig. 4. (A) Form factors for POPC (black line) with 0.02 mol fraction MA_{31} (red line) or $MA_{31}myr$ (blue line). Arrow indicates that $|F(q_z)|$ data shift to higher q_z values, indicating membrane thinning. (B) Total electron density profiles of samples shown in (A).

thickness, consistent with Fig. 6D, and increased the area/lipid, consistent with results in Fig. 6C. Addition of the peptide to the PS-containing bilayer had negligible effect on K_C, the hydrophobic thickness and area/lipid. As was the case for the data above, the results

are different for adding peptide to bilayers of PS- *vs.* PIP_2-containing lipids. While the responses of PC/PS mimics at this concentration (92:8 mol ratio) were smaller compared to those at 60:40 mol ratio, they were quite different from those of PC/PIP_2 (98:2 mol ratio),
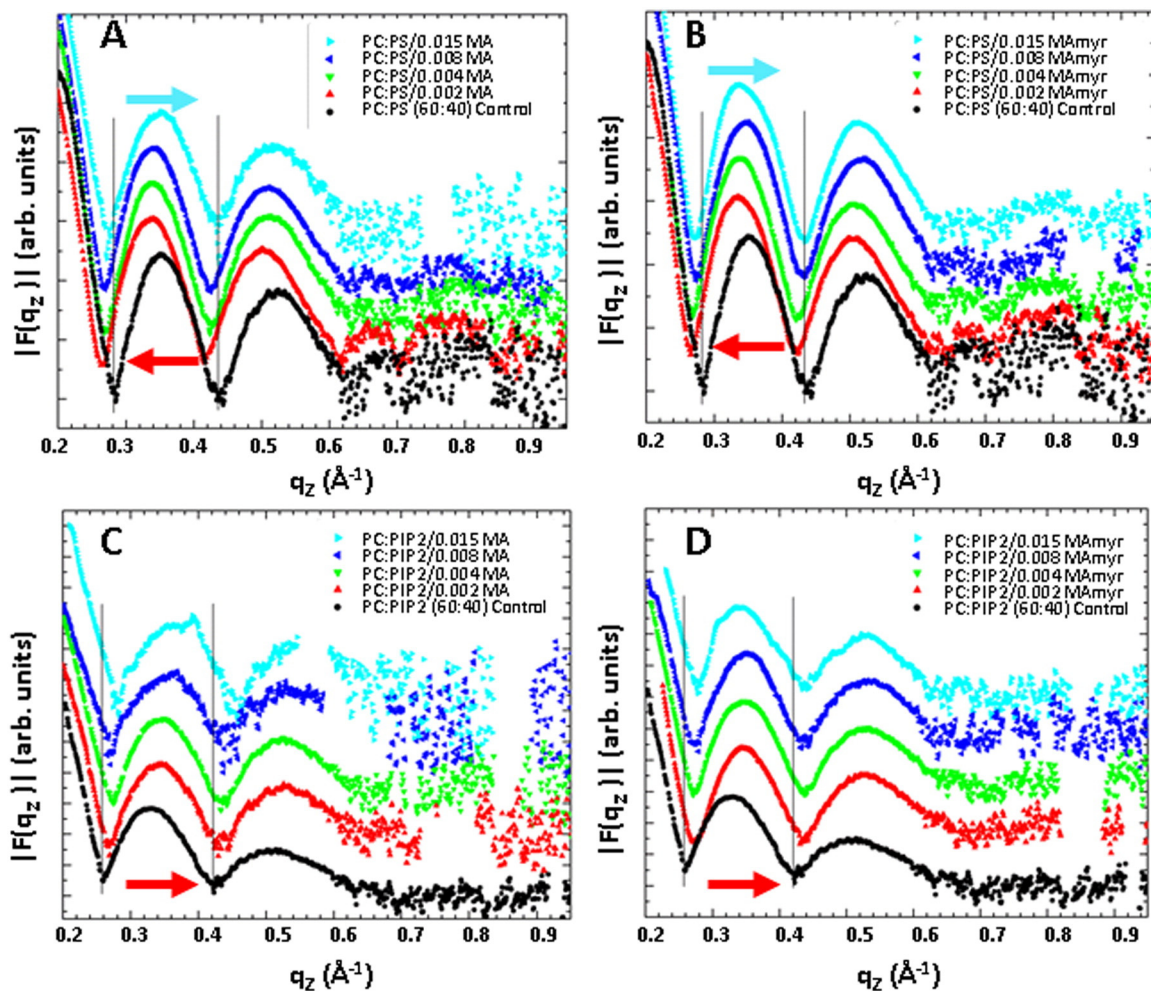
Fig. 5. Form factors as a function of lipid mimic and peptide mole ratio from 0 to 0.015 peptide/lipid. (A) MA_{31} in POPC/POPS (60:40 mol ratio), (B) $MA_{31}myr$ in POPC/POPS (60:40), (C) MA_{31} in POPC/PIP_2 (90:10), (D) $MA_{31}myr$ in POPC/PIP_2 (90:10). Arrows indicate membrane thickening (pointing to lower q_z values), and membrane thinning (pointing to higher q_z values). Control lipids are black solid circles in all sections. Form factors are shifted vertically for clarity.
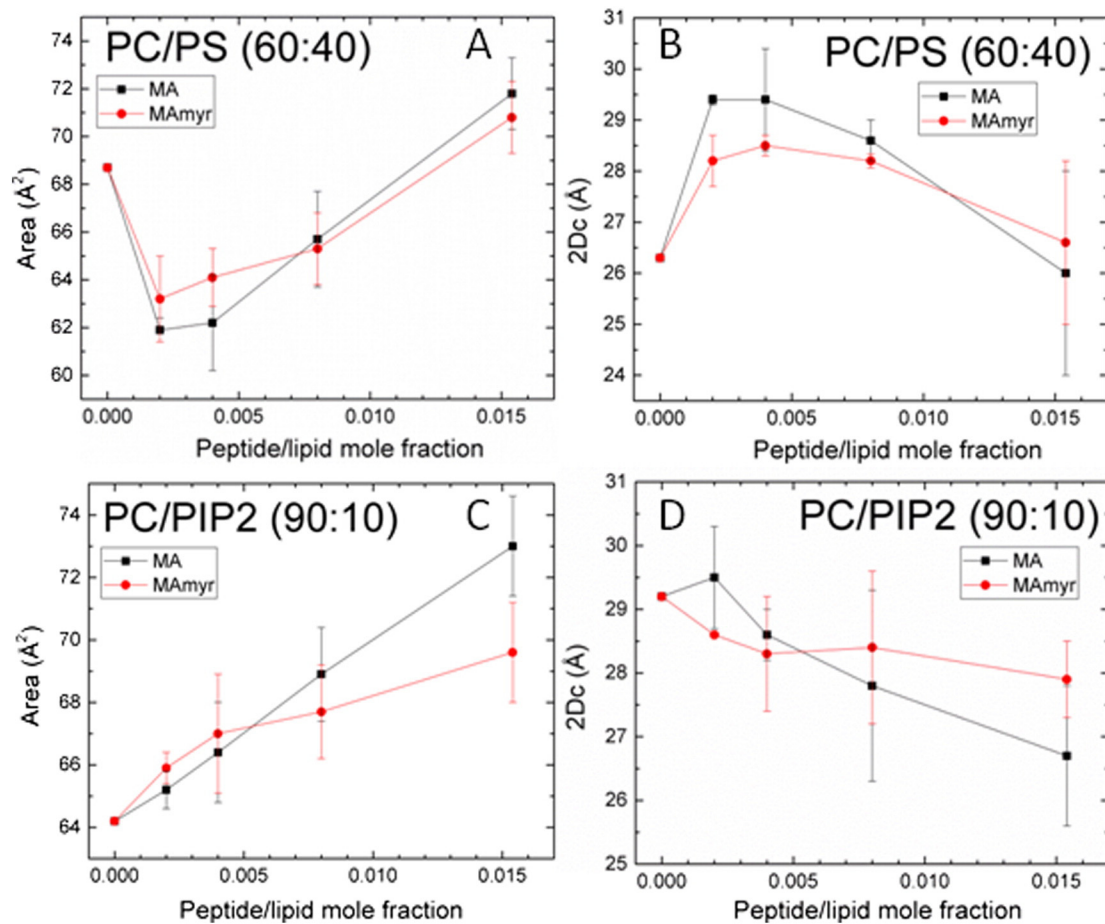
Fig. 6. Structural results vs. increasing peptide mole ratio: (A) area/lipid A_L in POPC/POPS (60:40), (B) hydrocarbon thickness $2D_C$ in POPC/POPS (60:40), (C) A_L in POPC/PIP$_2$ (90:10), (D) $2D_C$ in POPC/PIP$_2$ (90:10). Error bars indicate the standard deviations of the average of 2–5 fits.

suggesting that the results in Figs. 3D and 6 are in qualitative agreement with physiological concentrations of negatively charged lipids. We also note that it is the local responses that are important for functionality and these can be much larger than the measured responses which are averaged over the entire membrane.

The S_{xray} results shown in Fig. 8 for the samples in Table 2, also include additional samples containing POPE and cholesterol with the negatively charged lipids. Samples containing 30 mol% cholesterol had
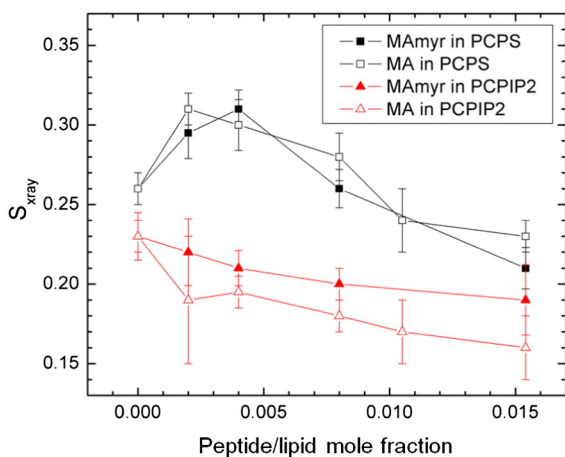
high S_{xray} values due to their increased chain order [48]. However, when 0.02 MAmyr was added to the mimic containing cholesterol and POPS, S_{xray} increased, while it decreased for the mimic containing cholesterol and PIP$_2$. This indicates that cholesterol does not interfere with the differences in chain order caused by PS *vs.* PIP$_2$. Similarly, when POPE was included, PS-containing samples increased, and PIP$_2$-containing samples decreased S_{xray} when MAmyr was added. Therefore, the changes caused by the peptide are dominated by their interactions with the negatively charged lipids, even at physiological concentrations. While it is true that the hydrocarbon chains in the lipids that we purchased from Avanti are different for POPS *vs.* porcine brain PI(4,5)P$_2$, we doubt that the additional polyunsaturation in the PIP$_2$ lipid plays a role in softening membranes. Indeed, we have found just the opposite [49].

Fig. 7. S_{xray} order parameter for MA$_{31}$myr or MA in POPC/POPS (60:40), or POPC/PIP$_2$ (90:10). S_{xray} values were corrected for misalignment of layers. Error bars indicate standard deviations from the average S_{xray} from 2 or more images.

Table 2
K_C and structural results for physiological lipid concentrations.

Membrane Mimic	K_C ($\times 10^{-20}$ J)	Std. Dev.	$2D_C$(Å)	Std. Dev.	Area/lipid (Å^2)	Std. Dev.
POPC	8.2	0.4	29.1	0.5	64	1
POPC/0.02 MAmyr	6.8	0.2	27.1	0.4	68.7	1.1
POPC/PIP$_2$(98:2)	7.6	0.1	29.6	0.6	63	1.1
POPC/PIP$_2$(98:2)/0.02 MAmyr	6.7	0.2	27.7	0.6	67.1	0.9
POPC/POPS(92:8)	6.0	0.2	27.8	0.4	67	0.8
POPC/POPS(92:8)/0.02 MAmyr	5.9	0.3	27.7	0.5	67.2	1.2

(For each membrane mimic, averages and standard deviations resulted from 2–10 samples.)
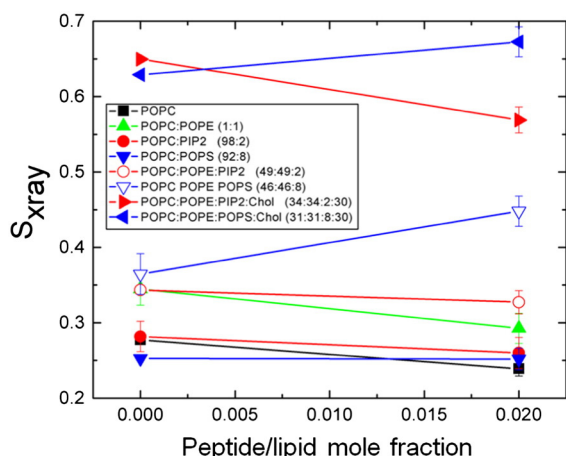
Fig. 8. S_{xray} order parameter for pure lipid mimetics and MA$_{31}$myr (see legend for lipid details). S_{xray} values were corrected for mosaic spread. Error bars represent standard deviation of average S_{xray} values from 2 to 4 images.

3.3. Neutron Reflectivity (NR)

While X-ray scattering is well suited to reporting changes in membrane thickness and elastic properties, neutron reflectivity is superior for obtaining peptide position in a bilayer due to greater contrast between the protein, lipid headgroup and lipid hydrocarbon chains [41]. NR results (Fig. 9) show MA$_{31}$myr located both in the headgroup (HG) region as well as 69 ± 17% in the hydrocarbon (HC) region in both membrane mimics. Within the 68% confidence limits, there were no significant differences between MA$_{31}$ and MA$_{31}$myr. See Fig. S3 for visualization of the 68% confidence limits.

3.4. D-spacing

The D-spacing of oriented samples as they were hydrated through the vapor phase either continuously increased, which we call D-unbound, or reached a limit, which we call D-bound. Instead of listing actual D-spacings, which were quite variable for the samples shown in Table 1 due to different effective relative humidity, the D-spacing is shown either as D-unbound or D-bound along with the overall net charge (based on a unit cell of one lipid plus the mole ratio of peptide and assuming a net charge of +7e on the peptides). At the highest MA$_{31}$myr concentration in both PC/PS and PC/PIP$_2$ membranes, the membranes became D-bound, similar to the condition for neutral lipid membranes. At the highest two MA$_{31}$ concentrations in PC/PIP$_2$ membranes, the membranes also became D-bound, but not in PC/PS membranes.

3.5. CD spectroscopy and volume measurements

CD spectroscopy for MA$_{31}$ and MA$_{31}$myr with several lipid mixtures are shown in Fig. S2. Similarly, volume results for MA$_{31}$ and MA$_{31}$myr in pure water and mixed with lipids are shown in Table S1.

Fig. 9. Scattering density profiles obtained from neutron reflectivity. A. POPC/POPS (60:40 mol ratio)/0.01 MA$_{31}$, B. POPC/POPS (60:40)/0.0125 MA$_{31}$myr, C. POPC/PIP$_2$ (90:10)/0.0125 MA$_{31}$, D. POPC/PIP$_2$ (90:10)/0.0125 MA$_{31}$myr. Bilayer components are shown in the legends; Gibbs dividing surfaces HC (green dashed line) and water (blue dashed line) are shown.

4. Discussion

4.1. Location of the peptides in the membrane mimics

A striking result, obtained from neutron reflectivity, is that the MA peptides reside more deeply in the interior of charged membrane mimics than one might have guessed, based on hydrophobicity scales [50]. *A priori*, such strongly positively charged peptides would have been predicted to occupy a more peripheral location, somewhat further from the center of the bilayer than the phosphate headgroups of the lipids. We propose that the deeper location can be understood in terms of the cartoon in Fig. 10 which shows a proposed distribution of the peptides along the membrane normal. This cartoon suggests that the charged amino acid side chains can be neutralized, thereby allowing greater hydrophobic penetration. Neutralization could be effected by the negatively charged lipids with those amino acids in the AA20–32 binding domain and by pairing and hydrogen bonding of positive and negative amino acids in AA2–19. If their charged ends are neutralized, lysine and arginine side chains are hydrophobic moieties.

It is interesting to relate our cartoon in Fig. 10 to recent paramagnetic relaxation enhancement studies of MA protein bound to bicelles [27]. The used 5-DOXYL-PC harbors an NMR perturbing nitroxyl radical at position 5 of the *sn*-2 stearoyl chain, which resides in the hydrocarbon region about 2–3 Å from the hydrocarbon/headgroup interface [51–54]. The largest perturbations were reported for G2, A3, R4, A5, S6 and L8, consistent with the placement of these residues in the hydrocarbon region in our Fig. 10. Some of the residues in the HBR were perturbed more than residues that are usually thought to reside outside the membrane; that is consistent with their residing in the headgroup region in Fig. 10.

Our interpretation may seem contrary to published neutron reflectivity results [6,55]. However, Ref. [55] used NR to study the non-myristoylated MA protein which was positioned at the surface of a bilayer containing saturated lipids. The results in Ref. [6] could be within the 68% confidence resolution of our present NR results (see Fig. S3). It may also be noted that the location of the peptides is relative to the average location of the lipids; at the local lateral position of the peptide, it would be possible for the lipid bilayer to be thinner, thereby placing the peptides less deeply into the hydrophobic core locally, as has previously been suggested for the HIV-1 Tat petide [56] and for the KvAP K + channel [57]. The mechanism for such thinning is that a peptide localized in the headgroup region will require the chains of
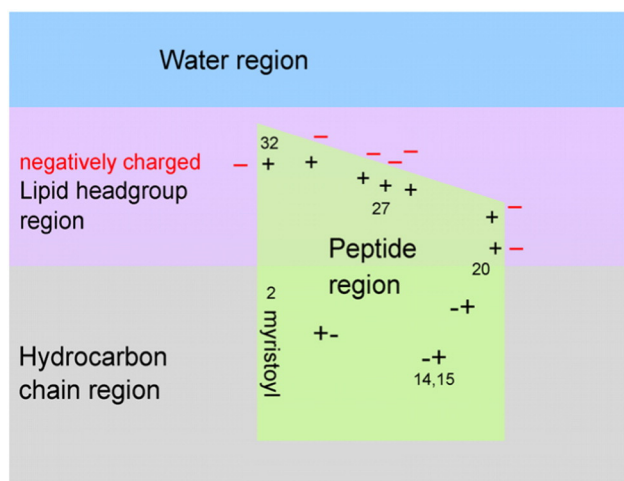
nearby lipids to fill in the hydrocarbon volume beneath the peptide; these chains will then be tilted, with a smaller projection along the bilayer normal, resulting in a locally thinner membrane. We note that the deep penetration of MA$_{31}$myr from our NR experiments do not agree with the much shallower penetration obtained from a coarse grained simulation of MA [58] that has not been validated against experimental structure involving a lipid bilayer. It is, of course, possible that the first 31 amino acids in the full MA reside less deeply in the membrane than our truncated peptides; the water soluble amino acids not included in our reductionist study might pull the binding sites towards the water. This conclusion would be supported if the same simulation methodology applied to MA$_{31}$myr agreed with our NR experimental results. Even if this is so, it is still of interest that our highly charged peptides reside so deeply in lipid bilayers.

4.2. PI(4,5)P$_2$ vs. PS

As was emphasized in the Introduction, PIP$_2$ is required for targeting of the precursor polyprotein, Pr55^{Gag}, to the PM, where the nascent virions acquire their lipid envelope from the local PM. We emphasize the importance of lipids by reporting differences between PIP$_2$ and PS at the membrane biophysical level as MA is added. The structural differences are shown in Fig. 6A and C for area/lipid, in Fig. 6B and D for membrane thickness, in Fig. 7 for chain order parameter S$_{xray}$, in Fig. S2 for circular dichroism and in Table 1 for the lamellar repeat spacing D. Structurally, the difference is that concentrations of both peptides thicken and order PS-containing membranes and thin and disorder PIP$_2$-containing membranes, although larger concentrations of peptides reverse the effect in PS-containing membranes. Decreasing the PC/PS lipid area and increasing the PC/PS membrane thickness by the peptides could result from the requirement for seven negatively-charged PS lipids to neutralize one peptide, which could compact the lipids near MA$_{31}$. Only two PIP$_2$ lipids are needed to neutralize MA$_{31}$, so compaction would not be as likely. While the secondary structures shown in Fig. S2 are not identical to the secondary structures in the intact MA protein [25], they are similar enough to warrant using this MA$_{31}$ binding domain to characterize MA/membrane interactions.

Structural differences, while clear, do not suggest functional differences. For that we turn to Fig. 3D which shows that the bending modulus K$_C$ becomes smaller when peptide binds to PIP$_2$-containing membranes and larger for PS-containing membranes. Making a membrane softer makes it easier to undergo the restructuring that is required for budding of the HIV-1 virion. The concentrations of MA peptides at which we find differences between PS and PIP$_2$-containing membranes are smaller than the concentration 0.03 MA/lipid in the fully formed immature virion [59]. We hypothesize that the lipid differences would be important during the recruitment of MA when its concentration is smaller than the upper bound of the fully formed virion. It is during this process that the membrane must bend substantially. While this is only one aspect of this complicated process, it is one that correlates our biophysical results well with functionality.

4.3. Myristoyl group

Since it has long been known that the myristoyl is involved in binding of Gag to the PM [60], we thought it was important for this biophysical study to test the effect of the myristoyl group by studying MA$_{31}$ in addition to MA$_{31}$myr. Surprisingly, our neutron reflectivity results show that both MA$_{31}$ and MA$_{31}$myr bound to and inserted deeply into both PS- and PIP$_2$- containing bilayers, suggesting that the myristoyl group might not have been needed. On the other hand, we may explain this surprising NR result as due to the large net charge in our membrane mimics that used more than the physiological concentration of PIP$_2$. Perhaps NR experiments on less charged systems, or with less peptide, would find differences between MA$_{31}$ and MA$_{31}$myr binding. We have obtained NR data using POPC tethered bilayers (not shown) that

Fig. 10. Cartoon representation of MA$_{31}$myr insertion into a negatively charged membrane, based upon neutron reflectivity results. The location of the 7 positively charged amino acid residues in the HBR from AA20–32 are visualized by + signs with nearby negatively charged lipid headgroups (− signs). The charged amino acids in the AA2–19 stretch are visualized as + − pairs. The last AA32 is visualized near bulk water to allow the remainder of the MA$_{131}$ protein to reside in water.

indicate no binding of either peptide. While this may appear to contradict our X-ray results that clearly show strong interaction with our peptides, there is no contradiction because there is roughly 10^5 times less water per lipid in the X-ray experiments, even though our X-ray samples consist of fully hydrated stacks with the order of 30 waters/lipid (~20 Å water between adjacent bilayers). Therefore, much more peptide becomes bound even with the same partition coefficient that gives negligible binding in the NR samples where there is ~0.2 mm of water on top of the tethered bilayer.

Also surprising at first glance, K_C of the neutral POPC bilayer decreased even more upon addition of MA_{31} than of $MA_{31}myr$, as seen in Fig. 3A. We suggest that both peptides are forced into the headgroup region of the neutral membranes in our X-ray samples, displacing lipid headgroups, creating a deficit pressure in the underlying hydrocarbon chain region, splaying the chains and thereby reducing K_C. The myristoyl chain on $MA_{31}myr$ would help fill in the hydrocarbon deficit region, thereby reducing K_C less compared to MA_{31}, as observed in Fig. 3A. Of course, binding would become stronger and deeper with a greater concentration of charged lipids, and differences between MA_{31} and $MA_{31}myr$ would be expected to disappear, consistent with our NR results in Fig. 8 and with our K_C results in Fig. 3C.

The D-spacing results in Table 1 are noteworthy with regard to both myristoylation and the lipids. First recall that electrostatic repulsion between neighboring membranes generally leads to D-unbinding. As the net negative charge is reduced by binding positively charged peptide to the lipids, the smaller electrostatic repulsion leads to D-binding, which is the usual state for systems of fully hydrated neutral bilayers. However, if the peptides do not bind or bind only partially, the electrostatic repulsion remains large and the stack of bilayers remains unbound. In this case, the peptides remain in the water space between membranes such as occurred with a positively charged monomer of the HIV-1 fusion peptide [36]. Less peptide binding in the MA_{31}/PS-containing system would account for MA_{31} remaining D-unbound at concentrations at which MA_{31}/PIP_2, $MA_{31}myr$/PS, and $MA_{31}myr$/PIP_2 became D-bound. The D-binding difference in Table 1 between MA_{31}/PS and MA_{31}/PIP_2 is consistent with specific binding of MA_{31} to PIP_2, and the difference between MA_{31}/PS and $MA_{31}myr$/PS is consistent with specific binding due to the myristoyl group.

5. Conclusions

Our first main conclusion is that many membrane properties are affected quite differently by the MA_{31} binding domain when PIP_2 lipids are replaced by PS lipids of equivalent charge. Of these membrane properties the one we hypothesize to be most likely to affect function is the bending modulus. Reducing this modulus reduces the free energy for restructuring the membrane for viral budding. Our result that the binding domain of MA_{31} reduces the bending modulus for the native PIP_2-containing membranes whereas it increases the bending modulus of the PS-containing membranes suggests another biological value for PIP_2 in addition to its recognized function of providing a stereo-specific anchor for the MA protein to the membrane [25].

In order to obtain this result we utilized 31 amino acid peptides that included the highly charged HBR in the membrane binding domain. Despite their high charge, our neutron reflectivity results show that a substantial portion of our peptides inserts quite deeply into the hydrocarbon interior when the lipid bilayer is highly charged. This second main result is consistent with our interpretation of recent NMR/spin label results for the entire myristoylated MA protein [27].

We also tested the effect of the myristoyl group by comparing $MA_{31}myr$ with MA_{31}. Our results implicate the myristoyl group as aiding MA_{31} binding only when a strong charge neutralization does not dominate the interaction. Overall, our results emphasize the importance of the lipid composition in MA_{31} peptide binding.

Appendix A. Supplementary data

Supplementary data to this article can be found online at http://dx.doi.org/10.1016/j.bbamem.2016.09.010.

References

[1] H.R. Gelderblom, E.H. Hausmann, M. Ozel, G. Pauli, M.A. Koch, Fine structure of human immunodeficiency virus (HIV) and immunolocalization of structural proteins, Virology 156 (1987) 171–176.
[2] V. Chukkapalli, A. Ono, Molecular determinants that regulate plasma membrane association of HIV-1 Gag, J. Mol. Biol. 410 (2011) 512–524.
[3] A. Ono, HIV-1 Assembly at the plasma membrane: Gag trafficking and localization, Futur. Virol. 4 (2009) 241–257.
[4] S.A.K. Datta, J.E. Curtis, W. Ratcliff, P.K. Clark, R.M. Crist, J. Lebowitz, S. Krueger, A. Rein, Conformation of the HIV-1 Gag protein in solution, J. Mol. Biol. 365 (2007) 812–824.
[5] J.B. Munro, A. Nath, M. Farber, S.A.K. Datta, A. Rein, E. Rhoades, W. Mothes, A conformational transition observed in single HIV-1 Gag molecules during in vitro assembly of virus-like particles, J. Virol. 88 (2014) 3577–3585.
[6] S.A.K. Datta, F. Heinrich, S. Raghunandan, S. Krueger, J.E. Curtis, A. Rein, H. Nanda, HIV-1 Gag extension: Conformational changes require simultaneous interaction with membrane and nucleic acid, J. Mol. Biol. 406 (2011) 205–214.
[7] N. Jouvenet, S.M. Simon, P.D. Bieniasz, Imaging the interaction of HIV-1 genomes and Gag during assembly of individual viral particles, Proc. Natl. Acad. Sci. U. S. A. 106 (2009) 19114–19119.
[8] S.B. Kutluay, T. Zang, D. Blanco-Melo, C. Powell, D. Jannain, M. Errando, P.D. Bieniasz, Global changes in the RNA binding specificity of HIV-1 Gag regulate virion genesis, Cell 159 (2014) 1096–1109.
[9] V. Chukkapalli, S.J. Oh, A. Ono, Opposing mechanisms involving RNA and lipids regulate HIV-1 Gag membrane binding through the highly basic region of the matrix domain, Proc. Natl. Acad. Sci. U. S. A. 107 (2010) 1600–1605.
[10] V. Chukkapalli, J. Inlora, G.C. Todd, A. Ono, Evidence in support of RNA-mediated inhibition of phosphatidylserine-dependent HIV-1 Gag membrane binding in cells, J. Virol. 87 (2013) 7155–7159.
[11] B. Olety, A. Ono, Roles played by acidic lipids in HIV-1 Gag membrane binding, Virus Res. 193 (2014) 108–115.
[12] W.J. Zhou, L.J. Parent, J.W. Wills, M.D. Resh, Identification of a membrane-binding domain within the amino-terminal region of Human-Immunodeficiency-Virus Type-1 Gag protein which interacts with acidic phospholipids, J. Virol. 68 (1994) 2556–2569.

[13] A. Ono, J.M. Orenstein, E.O. Freed, Role of the gag matrix domain in targeting human immunodeficiency virus type 1 assembly, J. Virol. 74 (2000) 2855–2866.

[14] C. Tang, E. Loeliger, P. Luncsford, I. Kinde, D. Beckett, M.F. Summers, Entropic switch regulates myristate exposure in the HIV-1 matrix protein, Proc. Natl. Acad. Sci. U. S. A. 101 (2004) 517–522.

[15] E.O. Freed, J.M. Orenstein, A.J. Buckler-White, M.A. Martin, Single amino acid changes in the human immunodeficiency virus type 1 matrix protein block virus particle production, J. Virol. 68 (1994) 5311–5320.

[16] A. Ono, E.O. Freed, Binding of human immunodeficiency virus type 1 Gag to membrane: Role of the matrix amino terminus, J. Virol. 73 (1999) 4136–4144.

[17] J.S. Saad, E. Loeliger, P. Luncsford, M. Liriano, J. Tai, A. Kim, J. Miller, A. Joshi, E.O. Freed, M.F. Summers, Point mutations in the HIV-1 matrix protein turn off the myristyl switch, J. Mol. Biol. 366 (2007) 574–585.

[18] J.C. Paillart, H.G. Gottlinger, Opposing effects of human immunodeficiency virus type 1 matrix mutations support a myristyl switch model of gag membrane targeting, J. Virol. 73 (1999) 2604–2612.

[19] S.A.K. Datta, L.G. Temeselew, R.M. Crist, F. Soheilian, A. Kamata, J. Mirro, D. Harvin, K. Nagashima, R.E. Cachau, A. Rein, On the role of the SP1 domain in HIV-1 particle assembly: a molecular switch? J. Virol. 85 (2011) 4111–4121.

[20] A. Ono, S.D. Ablan, S.J. Lockett, K. Nagashima, E.O. Freed, Phosphatidylinositol (4,5) bisphosphate regulates HIV-1 Gag targeting to the plasma membrane, Proc. Natl. Acad. Sci. U. S. A. 101 (2004) 14889–14894.

[21] F.D. Brown, A.L. Rozelle, H.L. Yin, T. Balla, J.G. Donaldson, Phosphatidylinositol 4,5-bisphosphate and Arf6-regulated membrane traffic, J. Cell Biol. 154 (2001) 1007–1017.

[22] M. Facke, A. Janetzko, R.L. Shoeman, H.G. Krausslich, A large deletion in the matrix domain of the human immunodeficiency virus gag gene redirects virus particle assembly from the plasma membrane to the endoplasmic reticulum, J. Virol. 67 (1993) 4972–4980.

[23] V. Chukkapalli, I.B. Hogue, V. Boyko, W.S. Hu, A. Ono, Interaction between the human immunodeficiency virus type 1 Gag matrix domain and phosphatidylinositol-(4,5)-bisphosphate is essential for efficient Gag membrane binding, J. Virol. 82 (2008) 2405–2417.

[24] R. Chan, P.D. Uchil, J. Jin, G.H. Shui, D.E. Ott, W. Mothes, M.R. Wenk, Retroviruses human immunodeficiency virus and murine leukemia virus are enriched in phosphoinositides, J. Virol. 82 (2008) 11228–11238.

[25] J.S. Saad, J. Miller, J. Tai, A. Kim, R.H. Ghanam, M.F. Summers, Structural basis for targeting HIV-1 Gag proteins to the plasma membrane for virus assembly, Proc. Natl. Acad. Sci. U. S. A. 103 (2006) 11364–11369.

[26] N. Shkriabai, S.A.K. Datta, Z.J. Zhao, S. Hess, A. Rein, M. Kvaratskhelia, Interactions of HIV-1 Gag with assembly cofactors, Biochemistry 45 (2006) 4077–4083.

[27] P.Y. Mercredi, N. Bucca, B. Loeliger, C.R. Gaines, M. Mehta, P. Bhargava, P.R. Tedbury, L. Charlier, N. Floquet, D. Muriaux, C. Favard, C.R. Sanders, E.O. Freed, J. Marchant, M.F. Summers, Structural and molecular determinants of membrane binding by the HIV-1 matrix protein, J. Mol. Biol. 428 (2016) 1637–1655.

[28] M. Barros, F. Heinrich, S.A.K. Datta, A. Rein, I. Karageorgos, H. Nanda, M. Lösche, Membrane binding of HIV-1 matrix protein: dependence on bilayer composition and protein lipidation, J. Virol. 90 (2016) 4544–4555.

[29] E.O. Freed, HIV-1 Gag proteins: diverse functions in the virus life cycle, Virology 251 (1998) 1–15.

[30] S.A. Tristram-Nagle, Preparation of oriented, fully hydrated lipid samples for structure determination using X-ray scattering, Methods Mol. Biol. 400 (2007) 63–75.

[31] N. Kučerka, Y.F. Liu, N.J. Chu, H.I. Petrache, S. Tristram-Nagle, J.F. Nagle, Structure of fully hydrated fluid phase DMPC and DLPC lipid bilayers using X-ray scattering from oriented multilamellar arrays and from unilamellar vesicles, Biophys. J. 88 (2005) 2626–2637.

[32] R. Budvytyte, G. Valincius, G. Niaura, V. Voiciuk, M. Mickevicius, H. Chapman, H.Z. Goh, P. Shekhar, F. Heinrich, S. Shenoy, M. Lösche, D.J. Vanderah, Structure and properties of tethered bilayer lipid membranes with unsaturated anchor molecules, Langmuir 29 (2013) 8645–8656.

[33] M.C. Wiener, S. Tristram-Nagle, D.A. Wilkinson, L.E. Campbell, J.F. Nagle, Specific volumes of lipids in fully hydrated bilayer dispersions, Biochim. Biophys. Acta 938 (1988) 135–142.

[34] Y.F. Liu, J.F. Nagle, Diffuse scattering provides material parameters and electron density profiles of biomembranes, Phys. Rev. E 69 (2004) 040901–040904(R).

[35] Y. Lyatskaya, Y.F. Liu, S. Tristram-Nagle, J. Katsaras, J.F. Nagle, Method for obtaining structure and interactions from oriented lipid bilayers, Phys. Rev. E 63 (2001) 0119071–0119079.

[36] S. Tristram-Nagle, R. Chan, E. Kooijman, P. Uppamoochikkal, W. Qiang, D.P. Weliky, J.F. Nagle, HIV fusion peptide penetrates, disorders, and softens T-cell membrane mimics, J. Mol. Biol. 402 (2010) 139–153.

[37] S. Tristram-Nagle, J.F. Nagle, HIV-1 fusion peptide decreases bending energy and promotes curved fusion intermediates, Biophys. J. 93 (2007) 2048–2055.

[38] M.S. Jablin, K. Akabori, J.F. Nagle, Experimental support for tilt-dependent theory of biomembrane mechanics, Phys. Rev. Lett. 113 (2014) 248102 (248101–248105).

[39] T.T. Mills, G.E.S. Toombes, S. Tristram-Nagle, D.M. Smilgies, G.W. Feigenson, J.F. Nagle, Order parameters and areas in fluid-phase oriented lipid membranes using wide angle X-ray scattering, Biophys. J. 95 (2008) 669–681.

[40] J.A. Dura, D.J. Pierce, C.F. Majkrzak, N.C. Maliszewskyj, D.J. McGillivray, M. Lösche, K.V. O'Donovan, M. Mihailescu, U. Perez-Salas, D.L. Worcester, S.H. White, AND/R: advanced neutron diffractometer/reflectometer for investigation of thin films and multilayers for the life sciences, Rev. Sci. Instrum. 77 (2006) 074301.

[41] F. Heinrich, M. Lösche, Zooming in on disordered systems: neutron reflection studies of proteins associated with fluid membranes, Biochim. Biophys. Acta Biomembr. 1838 (2014) 2341–2349.

[42] A.L. Boscia, K. Akabori, Z. Benamram, J.A. Michel, M.S. Jablin, J.D. Steckbeck, R.C. Montelaro, J.F. Nagle, S. Tristram-Nagle, Membrane structure correlates to function of LLP2 on the cytoplasmic tail of HIV-1 gp41 protein, Biophys. J. 105 (2013) 657–666.

[43] J.F. Nagle, K. Akabori, B.W. Treece, S. Tristram-Nagle, Determination of mosaicity in oriented stacks of lipid bilayers, Soft Matter 12 (2016) 1884–1891.

[44] D.L. Daleke, Regulation of phospholipid asymmetry in the erythrocyte membrane, Curr. Opin. Hematol. 15 (2008) 191–195.

[45] P.F. Devaux, Static and dynamic lipid asymmetry in cell membranes, Biochemistry 30 (1991) 1163–1173.

[46] Z.T. Graber, Z.P. Jiang, A. Gericke, E.E. Kooijman, Phosphatidylinositol-4,5-bisphosphate ionization and domain formation in the presence of lipids with hydrogen bond donor capabilities, Chem. Phys. Lipids 165 (2012) 696–704.

[47] J. Seelig, W. Niederberger, Deuterium-labeled lipids as structural probes in liquid-crystalline bilayers—deuterium magnetic-resonance study, J. Am. Chem. Soc. 96 (1974) 2069–2072.

[48] J.J. Pan, T.T. Mills, S. Tristram-Nagle, J.F. Nagle, Cholesterol perturbs lipid bilayers nonuniversally, Phys. Rev. Lett. 100 (2008) 198103 (198101–198104).

[49] N.V. Eldho, S.E. Feller, S. Tristram-Nagle, I.V. Polozov, K. Gawrisch, Polyunsaturated docosahexaenoic vs docosapentaenoic acid - Differences in lipid matrix properties from the loss of one double bond, J. Am. Chem. Soc. 125 (2003) 6409–6421.

[50] W.C. Wimley, S.H. White, Experimentally determined hydrophobicity scale for proteins at membrane interfaces, Nat. Struct. Biol. 3 (1996) 842–848.

[51] A. Chattopadhyay, E. London, Parallax method for direct measurement of membrane penetration depth utilizing fluorescence quenching by spin-labeled phospholipids, Biochemistry 26 (1987) 39–45.

[52] F.S. Abrams, E. London, Calibration of the parallax fluorescence quenching method for determination of membrane penetration depth: refinement and comparison of quenching by spin-labeled and brominated lipids, Biochemistry 31 (1992) 5312–5322.

[53] F.S. Abrams, A. Chattopadhyay, E. London, Determination of the location of fluorescent probes attached to fatty acids using parallax analysis of fluorescence quenching: effect of carboxyl ionization state and environment on depth, Biochemistry 31 (1992) 5322–5327.

[54] F.S. Abrams, E. London, Extension of the parallax analysis of membrane penetration depth to the polar-region of model membranes—use of fluorescence quenching by a spin-label attached to the phospholipid polar headgroup, Biochemistry 32 (1993) 10826–10831.

[55] H. Nanda, S.A.K. Datta, F. Heinrich, M. Losche, A. Rein, S. Krueger, J.E. Curtis, Electrostatic interactions and binding orientation of HIV-1 matrix studied by neutron reflectivity, Biophys. J. 99 (2010) 2516–2524.

[56] K. Akabori, K. Huang, B.W. Treece, M.S. Jablin, B. Maranville, A. Woll, J.F. Nagle, A.E. Garcia, S. Tristram-Nagle, HIV-1 Tat membrane interactions probed using X-ray and neutron scattering, CD spectroscopy and MD simulations, Biochim. Biophys. Acta Biomembr. 1838 (2014) 3078–3087.

[57] J.A. Freites, D.J. Tobias, G. von Heijne, S.H. White, Interface connections of a trans-membrane voltage sensor, Proc. Natl. Acad. Sci. U. S. A. 102 (2005) 15059–15064.

[58] L. Charlier, M. Louet, L. Chaloin, P. Fuchs, J. Martinez, D. Muriaux, C. Favard, N. Floquet, Coarse-grained simulations of the HIV-1 matrix protein anchoring: revisiting its assembly on membrane domains, Biophys. J. 106 (2014) 577–585.

[59] J.A.G. Briggs, H.G. Krausslich, The molecular architecture of HIV, J. Mol. Biol. 410 (2011) 491–500.

[60] W.J. Zhou, M.D. Resh, Differential membrane binding of the human immunodeficiency virus type 1 matrix protein, J. Virol. 70 (1996) 8540–8548.